Computers and Geotechnics xxx (xxxx) xxx–xxx

Contents lists available at ScienceDirect

Computers and Geotechnics

journal homepage: www.elsevier.com/locate/compgeo

Research Paper

A study of mode-I self-similar dynamic crack propagation using a lattice spring model

Gao-Feng Zhao[a,*], Kaiwen Xia[a,b]

[a] State Key Laboratory of Hydraulic Engineering Simulation and Safety, School of Civil Engineering, Tianjin University, Tianjin 300072, China
[b] Department of Civil Engineering, University of Toronto, Toronto M5S 1A4, Canada

ARTICLE INFO

Keywords:
Self-similar crack growth
Spontaneous fracture
Meso-mechanics
Distinct lattice spring model

ABSTRACT

The spontaneous crack growth in an infinite domain is studied using the distinct lattice spring model (DLSM). The kinetic energy, strain energy, crack opening, and crack branching during the crack growth are investigated numerically using a simple spring model. The discrete simulation satisfactorily reproduces the experimental observations and the theoretical predictions of the fracture energy increase even without considering the crack tip damage zone and crack bifurcation. Moreover, from analysis of the intrinsic fracture energy release rate, it was concluded that the observed fracture energy increase should originate from the distribution of kinetic energy during self-similar crack growth.

1. Introduction

According to Broberg, dynamic processes in a cracked body fall into two basic categories: dynamic crack propagation and dynamic loading of bodies with stationary cracks. Furthermore, virtually all known analytical solutions to elastodynamic crack propagation problems are based on either steady-state crack propagation or self-similarity models [5]. In the steady-state crack propagation model, the crack propagates at constant velocity, and the mechanical fields are invariant when the observer moving away or close to the crack tip [5,14]. The two-dimensional Yoffe problem refers to crack propagation of a pre-cracked body under far-field tensile loading [35]. In self-similar crack propagation, two crack tips move symmetrically at constant velocity from the crack initiation point, and the mechanical fields scale with the crack length. The steady-state crack propagation model was adopted in the pioneering paper series authored by Freund [10–13]. The model was widely accepted in the fracture mechanics community, partially because of the consistency of the notion of constant fracture energy or dynamic fracture toughness with that of static fractures. In fact, dynamic crack propagation is quite different from its static counterpart. For example, it was first shown by Rosakis et al. that fracture toughness continuously varies during crack growth, and thus, the dependence of fracture toughness on crack velocity was proposed [26]. The notion of constant fracture energy or dynamic fracture toughness was further challenged by the experiments performed by Ravi-Chandar and Knauss, who showed that there is no unique dependence of the fracture toughness on the propagation velocity [24]. The mystery of dynamic fracture propagation is thus far from resolved.

The key concept of self-similar crack propagation is that the mechanical fields are scaled with the crack length. Based on these assumptions, the time history of the dynamic stress intensity factor for mode-I self-similar crack propagation was first solved by Broberg [4] and thus, the problem was also referred to as Broberg's problem [33]. Subsequently, the analytical solution was further extended to an anisotropic solid [6] and mixed boundary conditions [30]. Contrary to steady-state crack propagation, in self-similar crack propagation, the fracture energy increases with the crack length [5]. This notion is inconsistent with that for static fractures, and as a result, the self-similar crack propagation model has received much less attention than the steady-state model.

However, recent progress has been reported on self-similar crack propagation. Under certain conditions, mode-I spontaneous fracture is found to be self-similar [33]. The concept of spontaneous fracture stems from earthquake physics [8,21] in which earthquake ruptures are modelled as spontaneous mode-II or mode-III fractures. Spontaneous fractures occur in a statically stressed domain, and after fracture initiation from a point, no external energy is supplied to the domain to further drive the fracture propagation. In addition to geophysics, the concept of spontaneous fracture also finds applications in engineering. Most engineering materials, such as the concretes, rocks, or even steels used in structures, have initial defects (e.g., microcracks) that are negligible in size compared with the entire structure, which is usually subjected to quasi-static loading. The failure of these defects might lead to a macro-scale catastrophic failure of the entire engineering structure.

* Corresponding author.
E-mail address: gaofeng.zhao@tju.edu.cn (G.-F. Zhao).

https://doi.org/10.1016/j.compgeo.2017.11.001
Received 23 April 2017; Received in revised form 12 October 2017; Accepted 3 November 2017

Therefore, a deeper insight into spontaneous crack propagation in solids is necessary to gain a better understanding of catastrophic failure [31,33,34].

If spontaneous mode-I fracture is initiated away from the boundary of the domain and the domain is sufficiently large, then at least the boundary conditions are satisfied for the Broberg's problem. By measuring the fracture velocity and the dynamic stress intensity factor using photoelasticity, the mode-I spontaneous fracture without the boundary effect was proven to be self-similar [33]. Until now, experimental evidence of self-similar mode-I crack propagation or approximately mode-I self-similar crack propagation has been identified for different materials, including plastics [3], steel [25], *Al/Sicp* [22], Homalite-100 and bonded PMMA [33]. These experimental results further confirm the Broberg theory for mode-I self-similar crack propagation [32]. As clearly measured using the photoelastic method [33], the fracture energy increases linearly with the crack length for mode-I spontaneous fracture. Thus, the question of interest is posed as follows: What is the mechanism for the increase in fracture energy? This question cannot be answered solely by experimental and theoretical means.

Due to the development of computer science, numerical simulation has become a promising complementary tool for the study of dynamic fracture problems. Generally, numerical methods can be classified into continuum-based methods and discrete element and lattice type methods [17]. Using numerical methods, the first clue to the mystery of the increase in the dynamic fracture energy was found by Johnson [18,19], who adopted the finite element method and represented the fracture process zone as a collection of cells. The numerical results published by Johnson [19] shown that the mode-I crack enlarges the process zone size to consume more energy rather than convert the strain energy into kinetic energy. Under high stresses, off-fault fracturing might be happen as demonstrated by Poliakov et al. [23] who conducted a numerical simulation of mode-II crack with a slip-weakening constitutive model.

This research suggested that the increase in the process zone size might be the mechanism underlying the increase in fracture energy during earthquake fracture propagation. Later numerical analysis by Andrews [2] showed in detail that the mode-II crack propagation in earthquakes is approximately self-similar and that the fracture energy is approximately proportional to the earthquake rupture length.

In discrete element and lattice type numerical methods such as the discrete element model (DEM), dynamic fracture can be simulated directly [36,37]. However, the main limitations of DEM are the determination of micro-scale parameters and the high computational cost [36]. Recently, the distinct lattice spring model (DLSM) [38] was developed to overcome these limitations. Many discrete element and lattice type numerical models are available, such as the Discrete Element Model (DEM) [7] and Peridynamics developed by Silling [27]. The Distinct Lattice Spring Model (DLSM) is an extension of the classical LSM [16] that was developed to overcome Poisson's limitation from introducing a multi-body shear spring. Certain literature reports are available on both the theories of and experiments on self-similar crack growth. However, it is not clear how the crack growth occurs. The fundamental requirement of such growth is that the fracture energy and thus the fracture toughness should increase with the crack length, which contradicts the traditional wisdom that fracture toughness is a material constant. Discrete element and lattice-type numerical methods offer a possible approach to further examination of the mechanism of many fracture phenomena. For example, the relationship between the crack speed and the creep and relaxation times was studied by [29] using a triangular lattice, dynamic crack propagation in a brittle material was investigated by Abraham [1] using an elastic-brittle triangle lattice, and crack nucleation was studied by Silling et al. [28] using the Peridynamics approach. The objective of this work is to further examine the mechanism of self-similar crack growth using the distinct lattice spring model (DLSM).

Compared with the classical DEM, the DLSM uses only half of the degrees of freedom, and therefore, the DLSM is much more computationally efficient than the DEM. Moreover, by introducing the multi-body shear spring, the DLSM is able to solve elastic dynamic problems with a full range of Poisson's ratio, which makes it a promising tool for the study of dynamic fracture problems. Indeed, the DLSM has been successfully applied for dynamic crack propagation in PMMA [20].

In this work, the DLSM was adopted to investigate the self-similar crack propagation problem. The context is organized as follows. First, a brief introduction to the DLSM is presented. The computational model used to simulate self-similar crack growth is described in detail, including the model setup, boundary conditions, and material parameter selection. The applicability of the DLSM to modelling of self-similar crack growth is proven by comparing the numerical results with the theoretical and experimental results from the crack speed of a self-similar crack and crack opening displacement (COD). The histories of the kinetic energy, strain energy, and damage zone around the crack tip are investigated numerically. Together with the numerical simulation results and the theoretical and experimental observations, selected conclusions on self-similar crack growth are derived.

2. Distinct Lattice Spring Model (DLSM)

The basic idea of the DLSM is to represent a solid using a group of mass particles with different sizes (for contact detection purpose) linked by the bonds of normal and shear springs. The major feature of the DLSM is that a multi-body shear spring was introduced to address the limitation of Poisson's ratio in classical lattice spring models [38]. Fig. 1 shows the corresponding computational model, calculation cycle, particle forces, and constitutive model in the DLSM. The lattice model is formed by linking two particles with a gap smaller than a given threshold value (see Fig. 1a).

The equation of motion of the mass particles and lattice network can be represented as

$$[\mathbf{K}]\mathbf{u} + [\mathbf{C}]\dot{\mathbf{u}} + [\mathbf{M}]\ddot{\mathbf{u}} = \mathbf{F}(t) \tag{1}$$

where $\mathbf{u}$ represents the vector of particle displacement, $[\mathbf{K}]$ is the stiffness matrix, $[\mathbf{M}]$ is the diagonal mass matrix, $[\mathbf{C}]$ is the damping matrix, and $\mathbf{F}(t)$ is the vector of external force. In the DLSM, Eq. (1) is solved using the explicit central finite difference scheme. One calculation cycle is shown in Fig. 1b. Given the particle displacements, new contacts and broken bonds are detected. Particle forces (see Fig. 1c) can be obtained from the contact and spring forces between particles, which are updated according to the force-displacement relations, as shown in Fig. 1d. The particle velocity is obtained as

$$\dot{\mathbf{u}}_i^{(t+\Delta t/2)} = \dot{\mathbf{u}}_i^{(t-\Delta t/2)} + \frac{\sum \mathbf{F}_j^{(t)}}{m_p}\Delta t \tag{2}$$

where $\dot{\mathbf{u}}_i^{(t+\Delta t/2)}$ is the particle velocity at $t + \Delta t/2$, $\dot{\mathbf{u}}_i^{(t-\Delta t/2)}$ is the particle velocity at $t-\Delta t/2$, m_p is the particle mass, $\sum \mathbf{F}_j^{(t)}$ is the sum of contact forces acting on the particle i including applied external forces, and Δt is the time step. Finally, the new displacement of the particle is calculated as

$$\mathbf{u}_i^{(t+\Delta t)} = \mathbf{u}_i^{(t)} + \dot{\mathbf{u}}_i^{(t+\Delta t/2)}\Delta t \tag{3}$$

where $\mathbf{u}_i^{(t+\Delta t)}$ is the displacement at $t + \Delta t$, and $\mathbf{u}_i^{(t)}$ is the displacement at t.

In the DLSM, the normal spring was implemented as in the classical lattice spring model. For a bond that connects particle i and particle j, the normal unit vector $\mathbf{n} = (n_x, n_y, n_z)^{\mathrm{T}}$ pointing from particle i to particle j is defined. The relative displacement between two particles can be obtained as

$$\mathbf{u}_{ij} = \mathbf{u}_j - \mathbf{u}_i \tag{4}$$

The normal deformation of the spring is defined as

$$\mathbf{u}_{ij}^n = (\mathbf{u}_{ij} \cdot \mathbf{n})\mathbf{n} \tag{5}$$

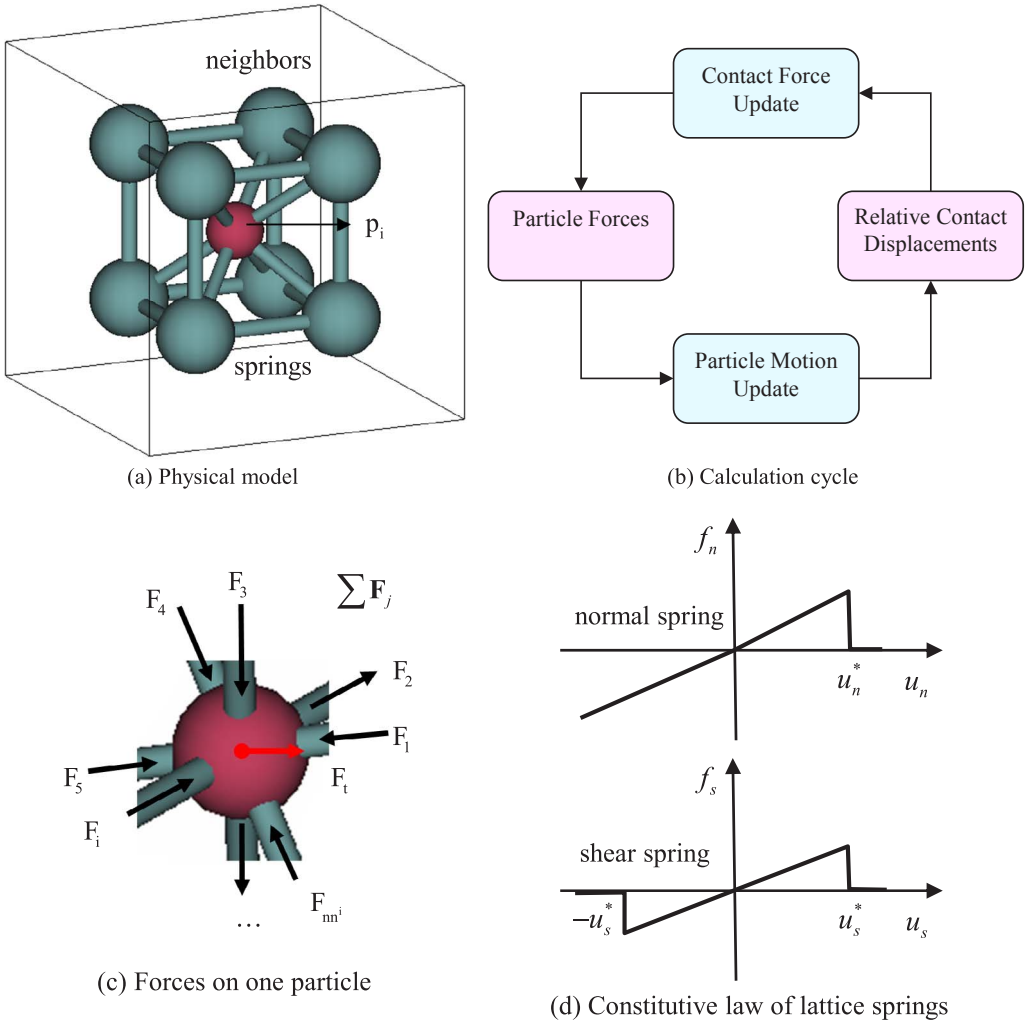

(a) Physical model

(b) Calculation cycle

(c) Forces on one particle

(d) Constitutive law of lattice springs

Fig. 1. Basic principle of the DLSM [38].

The normal force between the two particles is given as

$$\mathbf{F}_{ij}^{n} = k_n \mathbf{u}_{ij}^{n} \tag{6}$$

where k_n is the stiffness of the normal spring.

The shear spring was introduced to model the multi-body non-central interaction. The relative shear deformation is calculated using a local strain method as

$$\hat{\mathbf{u}}_{ij}^{s} = [\varepsilon]_{bond}\mathbf{n}l - (([\varepsilon]_{bond}\mathbf{n}l)\cdot\mathbf{n})\mathbf{n} \tag{7}$$

where l is the initial bond length, $[\varepsilon]_{bond} = \frac{[\varepsilon]_i + [\varepsilon]_j}{2}$ is the strain state of the connecting bond, and the strains at the two particles are represented as $[\varepsilon]_i$ and $[\varepsilon]_j$, which are evaluated using a least squares method [38]. The shear force between the two particles is given as

$$\mathbf{F}_{ij}^{s} = k_s \hat{\mathbf{u}}_{ij}^{s} \tag{8}$$

where k_s is the stiffness of the shear spring.

The constitutive model used in the DLSM is shown in Fig. 1d. For the tensile loading conditions considered in this work, only the failure of a normal spring is considered. When the normal displacement of the bond exceeds the prescribed value, the bond is broken and becomes a contact (a normal spring with zero strength). For elastic brittle problems, only one failure parameter exists in the DLSM, and this parameter can be easily calibrated. For static problems, the mechanical damping [38] is used, which can be written as

$$\dot{\mathbf{u}}_i^{(t+\Delta t/2)} = \dot{\mathbf{u}}_i^{(t-\Delta t/2)} + \{\sum \mathbf{F}_j^{(t)} - \alpha|\sum \mathbf{F}_j^{(t)}|\mathrm{sgn}(\dot{\mathbf{u}}_i^{(t-\Delta t/2)})\}\frac{\Delta t}{m_p} \tag{9}$$

where α is the damping constant (set to 0.2 in this paper). Additional details on the DLSM can be found in Ref. [38].

3. Numerical model for “self-similar growth”

The DLSM is used to simulate the ideal “self-similar” crack growth test conducted by Xia et al. [33]. The test setup is illustrated in Fig. 2. An exploding wire technique was used to initiate the spontaneous dynamic fracture (see Fig. 2a). During the test, the far-field quasi-static tensile loading was first loaded to a desired stress level, and the stored strain energy drove the subsequent dynamic crack propagation trigged by the explosion. A high-speed camera was used to capture the real-time isochromatic fringe patterns (see Fig. 2b), which were subsequently used to obtain the crack-tip position, crack propagation velocities, and dynamic stress intensity factor [33].

3.1. Numerical model

The key to the numerical simulation using the DLSM is to load the sample statically and initiate the dynamic fracture propagation in the centre of the sample. A two-stage calculation scheme is adopted (see Fig. 3). In the first stage (Fig. 3a), a static calculation with mechanical damping was performed, and the displacement field was recorded to a file. In the second stage, this file was inputted as the initial condition for the dynamic calculation. Note that the boundary conditions of the two stages are different (see Fig. 3b).

For the static loading, a tensile force was applied on the top surface

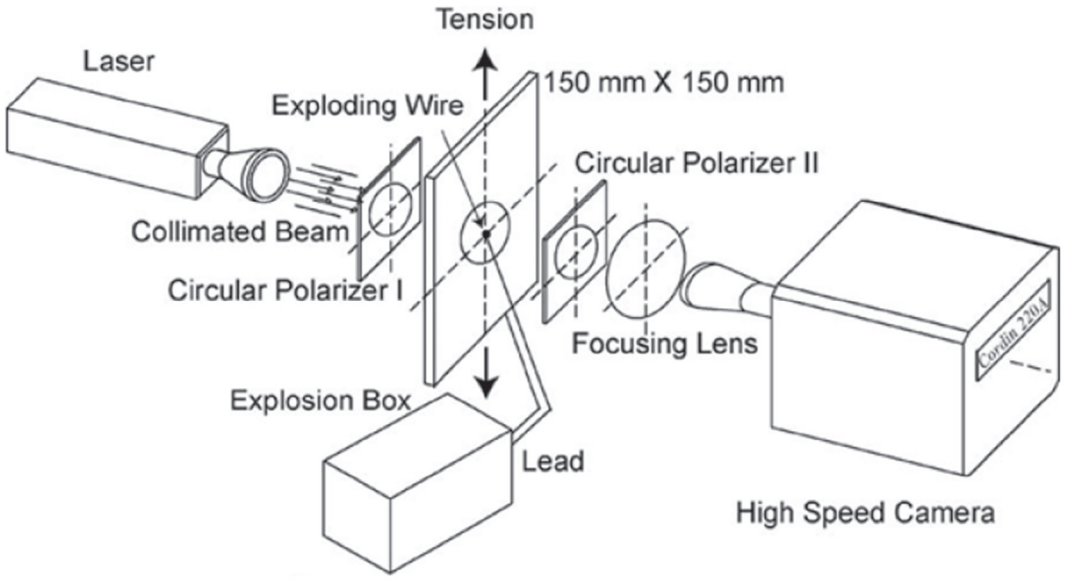

(a) Experimental set up

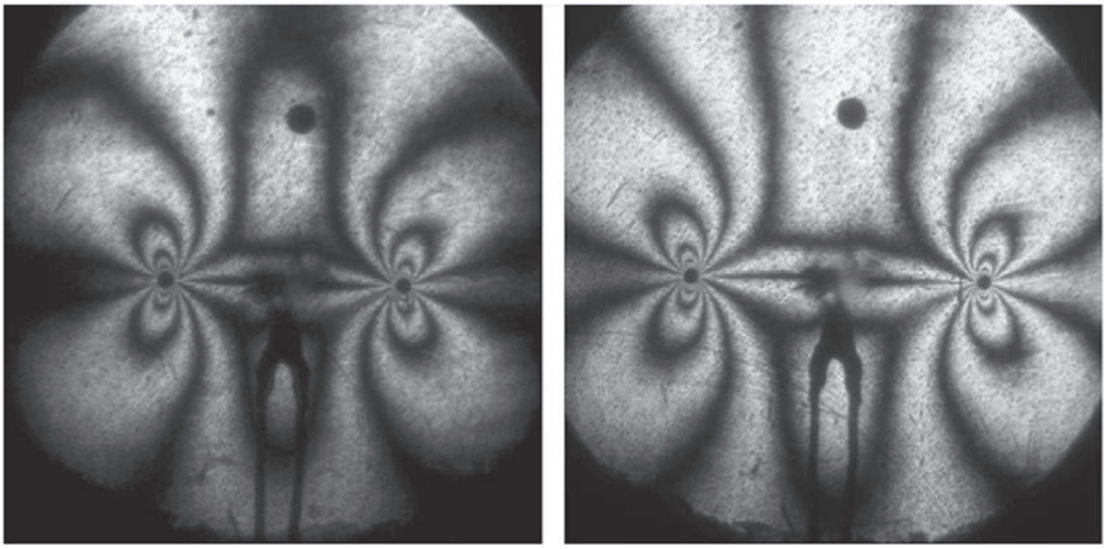

(b) Isochromatic fringes of propagating crack in Homalite-100

Fig. 2. Ideal "self-similar" crack growth test conducted by Xia et al. [31,33].

of the specimen, whereas the top surface was fixed in the dynamic calculation to ensure that the model is an isolated one. The computational model is shown in Fig. 3c. A thin-layer model was used to simulate the plane stress problem using the DLSM (a three-dimensional code). To save computational time, only two layers of particles exist along the out-of-plane direction. The dimensions of the numerical specimen are 300 mm × 300 mm. The numerical specimen consists of 180,000 particles with a diameter of 1 mm (see Fig. 3c). Note that the particle size in the DLSM is much larger than the actual molecular size of Homalite-100. The main purpose of the larger particle size is to reduce the computational time and to replace the complex molecular potential function with a simplified spring constitutive law. As shown in Fig. 3c, the particle is nearly invisible at the model scale. To show the pre-crack surface and the actual particle, an enlarged 3D view is presented in Fig. 3d. The pre-crack surface was formed by cutting the spring bonds that intersect the crack surface, which results in spontaneous dynamic fracture, as required in the ideal "self-similar" crack growth test. The following material parameters were taken from [33] to represent Homalite-100: Young's modulus of 3860 MPa, Poisson's ratio of 0.35, and density of 1230 kg/m^3.

3.2. Crack speed

In this section, the DLSM is verified against the experimental and theoretical results presented in Ref. [32]. The theoretical relationship between the crack speed and the loading parameter is shown in Fig. 5, as modified from Ref. [32]. Mathematically, the relationship is represented as

$$\frac{\sigma^{\infty}}{\sigma_0} = f\left(\frac{V}{C_R}\right) \tag{10}$$

where σ^{∞} is the far-field quasi-static tensile loading, σ_0 is an undetermined parameter related to the cohesion strength [15], V is the crack speed, and C_R is the Rayleigh wave speed. Details of the mathematic expression of f can be found in the literature [32]. In this work, for numerical modelling using the DLSM, the loading parameter is

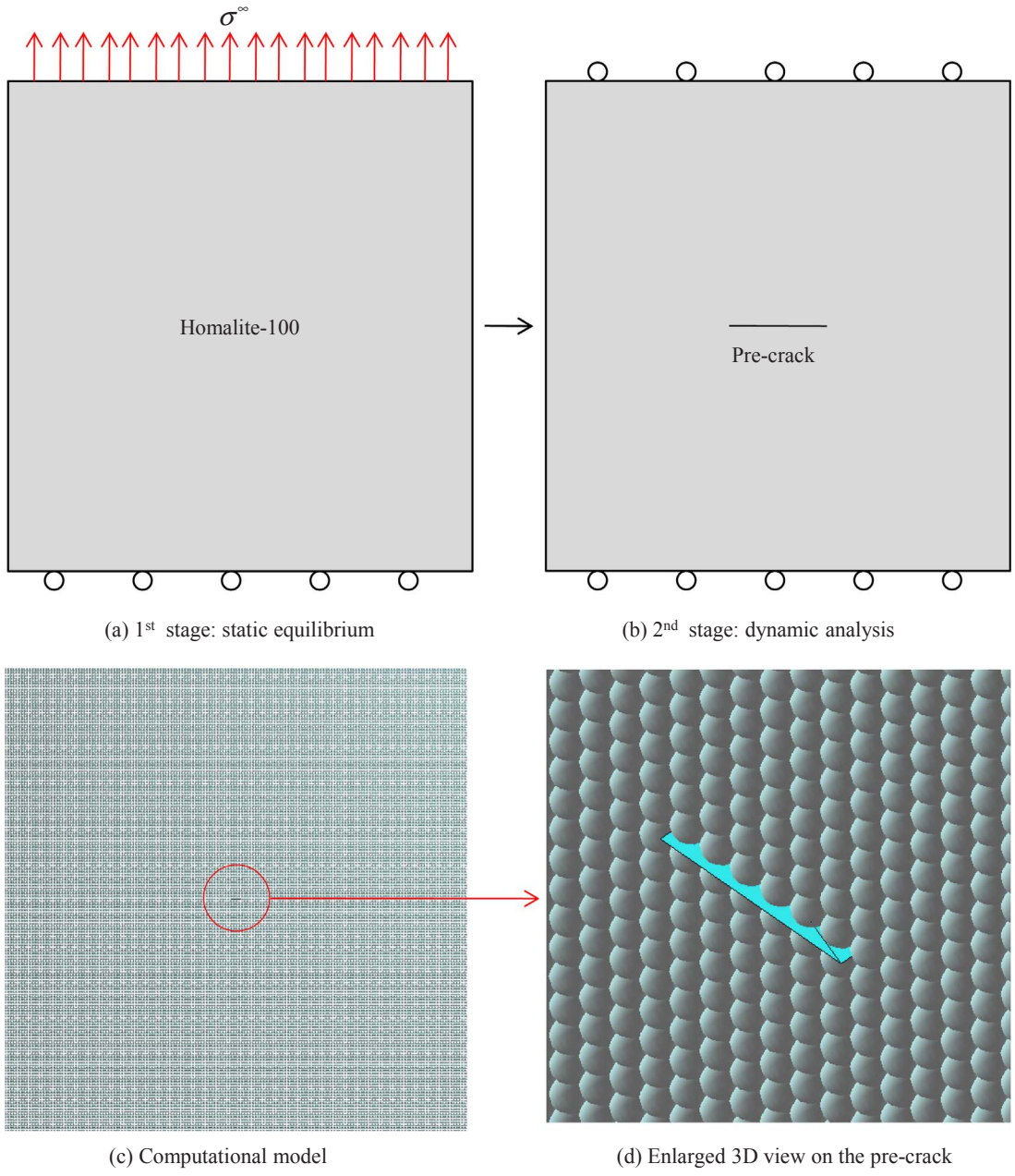

Fig. 3. Numerical model of the ideal "self-similar" crack growth test using the DLSM.

further expressed as

$$\frac{\sigma^{\infty}}{\sigma_0} = \frac{\sigma^{\infty}/E}{\sigma_0/E} = \frac{\varepsilon^{\infty}}{\varepsilon_0} \tag{11}$$

where E is the elastic modulus, and ε^{∞} is the uniform quasi-static strain that can be calculated as $\varepsilon^{\infty} = \frac{u^{\infty}}{L}$ in the DLSM. In the above expression, u^{∞} is the pre-applied tensile deformation at the top surface, L is the model size, and ε_0 is the cohesion strain related parameter given by

$$\varepsilon_0 = \frac{u_n^*}{\lambda d} \tag{12}$$

where λ is a scale parameter, d is the particle size (1 mm), and u_n^* is the ultimate deformation of the spring bond.

Substituting Eq. (12) into Eq. (11), the loading coefficient can be expressed as

$$\frac{\sigma^{\infty}}{\sigma_0} = \lambda \frac{u^{\infty}/L}{u_n*/d} \tag{13}$$

The parameter λ can be determined from the crack speed predicted by the numerical simulation and the corresponding input material parameters as $\lambda = \frac{u_n*}{u^{\infty}/L} f\left(\frac{V}{C_R}\right)$ (in this work, $\lambda = 3$). Fig. 4 shows a numerical simulation of self-similar crack growth using the DLSM ($u_n* = 0.012$ mm).

The crack speed is obtained from a linear fitting of the history of the half crack length over time. Different loading parameters and crack speeds can be obtained by setting different tensile failure parameters u_n*. The results predicted using the DLSM are plotted in Fig. 5 together with the theoretical and experimental results [32]. The numerical results agree well with the theoretical and experimental results. In this work, the plot of the relation between fracture energy and the crack length is plotted as the total length of the crack such that the slope directly corresponds to the fracture energy release rate. Additionally, when a figure is used to indicate the crack propagation, a half crack is preferable such that the slope directly corresponds to the crack speed.

In a discrete simulation, the particle size should be treated as a

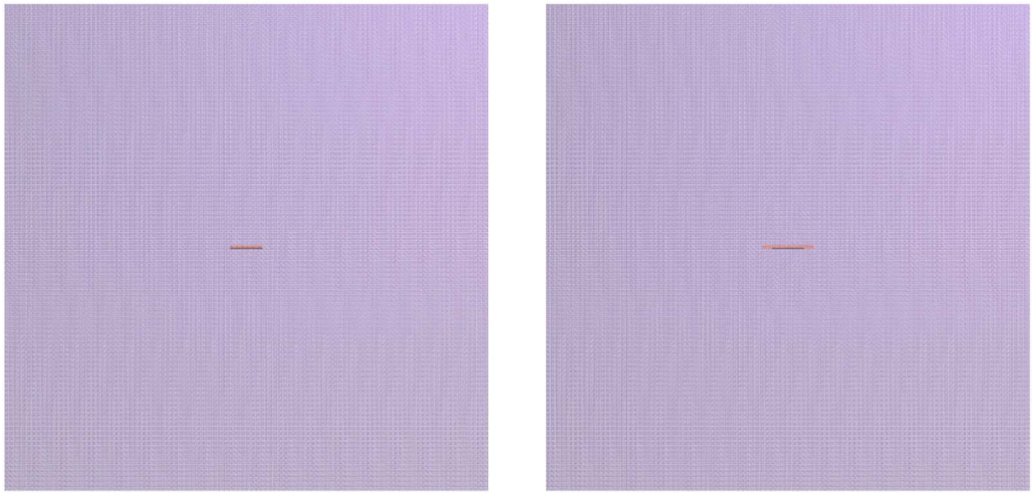

(a) t = 3 μs (b) t = 30 μs

(c) t = 51 μs (d) t = 81 μs

Fig. 4. "Self-similar" crack growth predicted by the DLSM (red colour refers to broken particles). (For interpretation of the references to colour in this figure legend, the reader is referred to the web version of this article.)

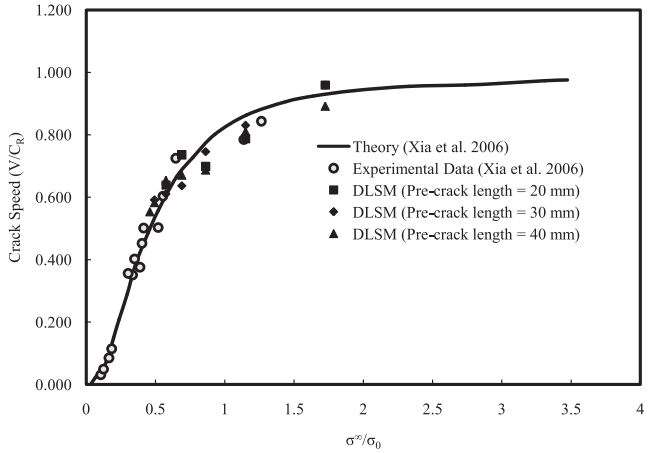

Fig. 5. Comparison of the numerical results using the DLSM and the theoretical and experimental results [32].

relative parameter, and its influence on the simulation depends on the scale of the problem. In Fig. 5, discrete models with different pre-crack lengths (problem size) were used to model self-similar crack growth. The results are found to be similar, and the current choice of particle size is sufficiently small. Therefore, the physical reality of the simulation is influenced by the particle size chosen in the current work.

3.3. Crack opening displacement

In fracture mechanics, the stress intensity factor can be obtained using the displacement extrapolation method

$$K_I = \lim_{r\to 0} A\frac{COD(r)}{\sqrt{r}} \tag{14}$$

where A is a constant related to the elastic modulus and Poisson's ratio, r is the distance from the crack tip, and $COD(r)$ is the crack tip opening displacement at r. The crack tip opening displacements of a numerical model ($u^{\infty} = 0.7$ mm, $u_n* = 0.012$ mm, pre-crack length = 20 mm) are shown in Fig. 6.These COD curves are found to be self-similar. Assuming a state with a half-crack length of 1 mm, the corresponding stress intensity factor is

$$K_I^0 = \lim_{r^0\to 0} A\frac{COD^0(r^0)}{\sqrt{r^0}} \tag{15}$$

If the half-crack length is x, using the variable substitution method and the COD function in Fig. 6, the stress intensity factor can be calculated as

$$K_I^x = \lim_{r^x\to 0} A\frac{COD(r^x)}{\sqrt{r^x}} = \lim_{r^0\to 0} A\frac{xCOD^0(r^0)}{\sqrt{xr^0}} = \sqrt{x}K_I^0 \tag{16}$$

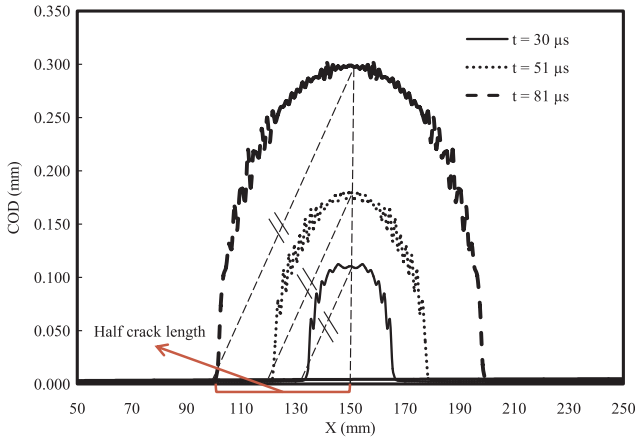

Fig. 6. Crack opening displacement of self-similar crack growth predicted using the DLSM ($u_n^* = 0.012$ mm, pre-crack length = 20 mm).

Eq. (16) is written in the same form as Eq. (4) in Ref. [33], but it is based solely on the numerical observation. This result indicates that the stress intensity factor reproduced by the DLSM also agrees with the theoretical and experimental observations [33].

From the above results, it is concluded that the DLSM is able to model the self-similar crack growth problem. Note that the numerical results obtained using different pre-crack lengths do not change the results (see Fig. 5). This observation is consistent with the concept of self-similar crack growth. Because the size of the crack is a relative value from the perspective of the observer, the initial crack becomes smaller as the observer moves away from the centre point. However, the crack speed should not change. In the following, the DLSM is further used to obtain deeper insight into self-similar crack growth.

4. Numerical results and discussion

4.1. Fracture energy analysis

4.1.1. Crack propagation is not permitted

The spontaneous fracture induces stress waves in the model. If the normal failure parameter is sufficiently large, then crack propagation cannot be initiated. As shown in Fig. 7, the pre-crack generates both P and S waves from the crack tip that propagate to the model boundary. This wave propagation induces a variation in the kinetic energy within the model. Two characteristic times are used in the modelling: the first time is the arrival of the P wave at the model boundary (66.8 μs), and the second time is the arrival of the reflected P wave back at the crack surface (133.8 μs).

The modelling results before the first characteristic time fully satisfy the conditions (crack growth and energy distribution) of self-similar crack growth. Before the second characteristic time, the reflected wave does not interact with the crack. The crack growth should be the same as that of a self-similar crack, whereas the energy should not be the same. After the second characteristic time, both the crack growth and the energy distribution are affected.

To show the change in the kinetic energy of the model, the pre-crack induced kinetic energy of the model for pre-cracks of different lengths is shown in Fig. 8. A longer pre-crack length induces a larger kinetic energy (see Fig. 8). Before the arrival of the induced wave at the model boundary, the kinetic energy enters a relatively stable range.Fig. 9 shows the results of the calculations of the strain energy in these models. The released strain energy of a model is defined as

$$\Delta U(t) = U^0 - U(t) \tag{17}$$

where U^0 is the total strain energy of the model before cracking, and $U(t)$ is the strain energy of the model at time t. Fig. 10 shows the results of the released energy of models with different pre-crack lengths at different times under the static condition (mechanical damping is applied). At the initial stage (t = 0 μs), the released strain energy is proportional to the length of the pre-crack, whereas a quadratic relationship with the length of the pre-crack is observed at t = 12, 47, and 147 μs for a group of roughly dynamic stable values (see Fig. 10).Because the fracture energy defined by the strain energy release rate is given as

$$G = \frac{\Delta U}{\partial L} \tag{18}$$

the fracture energy release rate G of the quadratic fitting in Fig. 10 is a linear function of the crack length. The intrinsic fracture energy should be defined as

$$\Delta U^{FI}(t) = \Delta U(t) - E(t) \tag{19}$$

where $E(t)$ is the kinetic energy of the model at time t. For a closed system without any cracks, the fracture energy should be zero, and for a cracked system, the energy is purely due to the presence of the crack. Therefore, we refer to this quantity as the intrinsic fracture energy. The variation in the intrinsic fracture energy of the models with different pre-crack lengths is shown in Fig. 11. It should be mentioned that the strain energy lost when t = 0 is due to the spontaneous cut of the pre-crack. Under the static condition, the intrinsic fracture energy is equal to the released strain energy. The intrinsic fracture energy under the dynamic condition is much less than the released strain energy. After the stable time instances (t = 12, 47, and 147 μs), the intrinsic fracture energy is nearly negligible.

4.1.2. Crack propagation is permitted

When crack propagation is allowed ($u_n^* = 0.012$ mm), the strain and kinetic energies of the model with a pre-crack length of 20 mm are illustrated in Fig. 12. The released energy of the model is shown in Fig. 13. The released strain energy can be fitted using a power function as

$$\Delta U(t) = aL^b \tag{20}$$

The fitting coefficient b is 2.024.

In this work, the reason for the choice of DLSM is that it is a numerical model based on basic physical theorems, i.e., Newton's second law and Hooke's law, and therefore, the simulation results based on the model are simpler and more straightforward. The analysis in Section 3.3 reproduces the increase in the critical intensity factor (corresponding to the fracture energy release rate G) obtained from photoelastic analysis in the experiment of Xia et al. [31,33]. In this section, the corresponding fracture energy release rate G of the numerical simulation is roughly proportional to the crack length, which is consistent with the observation of Xia et al. [31,33] as well. Because our numerical simulation did not consider the crack tip damage zone and crack bifurcation, we conclude that the damage zone and crack branching observed in the experiment might not be the source of the fracture energy increase. Moreover, as shown in Fig. 13, the intrinsic fracture energy release rate of the model is constant. Together with the definition of the intrinsic fracture energy (Eq. (19)), the observed fracture energy increase should originate from E(t), i.e., the distribution of kinetic energy during self-similar crack growth.

4.2. Energy dissipation under different far-field loadings

In the verification section, the loading parameter was adjusted by changing the material parameter u_n^*, whereas the far-field loading u^∞ was held constant at 0.7 mm. In this section, the far-field loading was reduced to 0.35 mm. To obtain the same loading parameter, the material parameter was reduced to 0.006 mm. According to the theoretical prediction of self-similar crack growth, the crack speed predicted by the two numerical simulations should be the same. Our simulation results reproduced this phenomenon successfully (Fig. 14). The half-crack

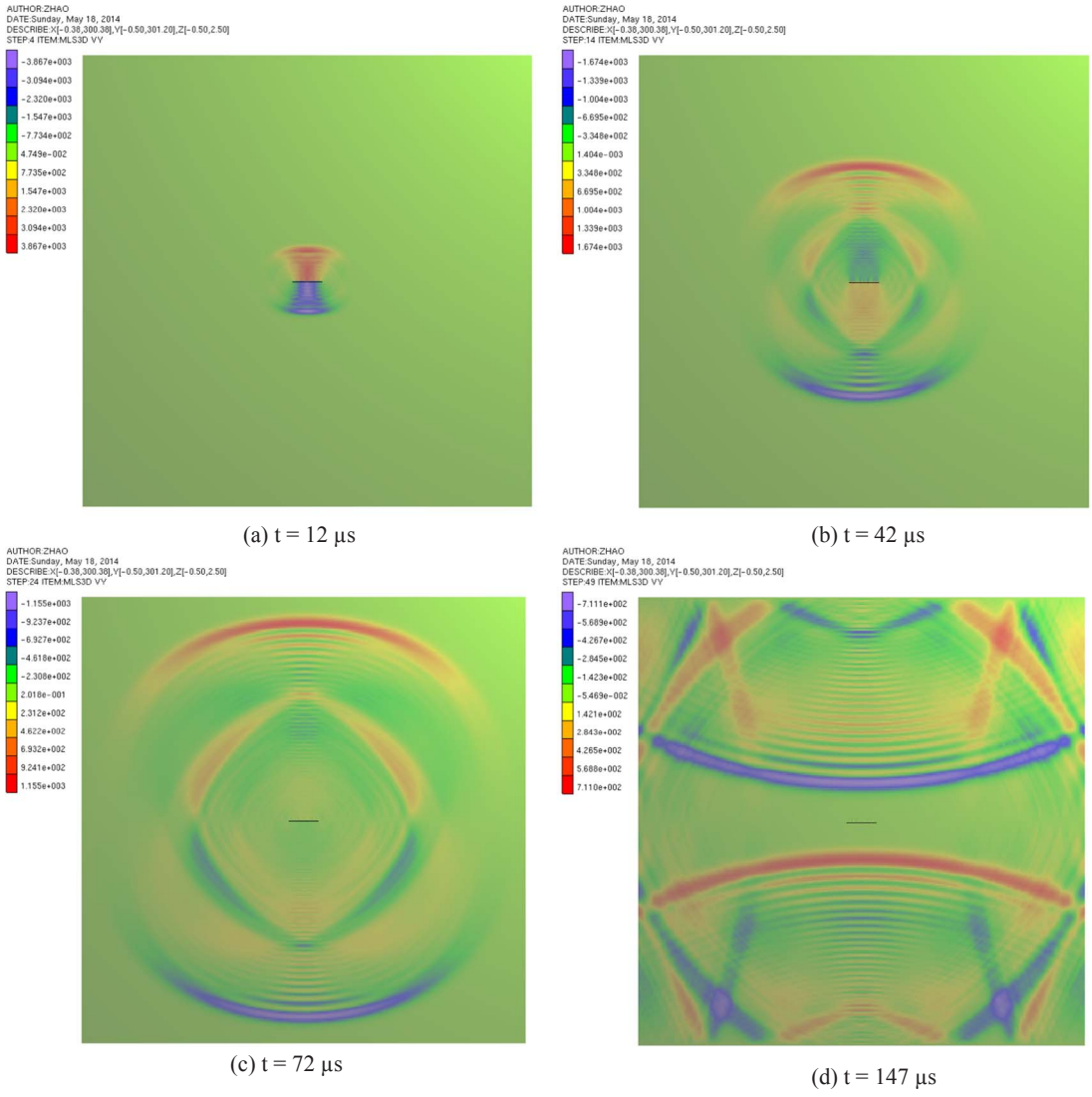

Fig. 7. Strain wave induced by the spontaneous crack in a pre-loaded specimen.

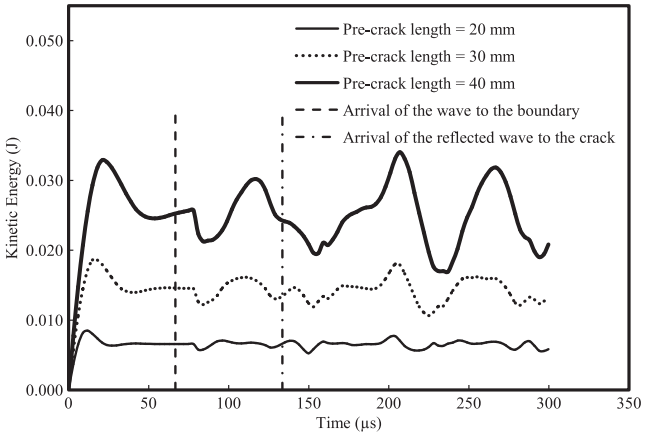

Fig. 8. Kinetic energy of models with different pre-crack lengths (crack propagation not allowed).

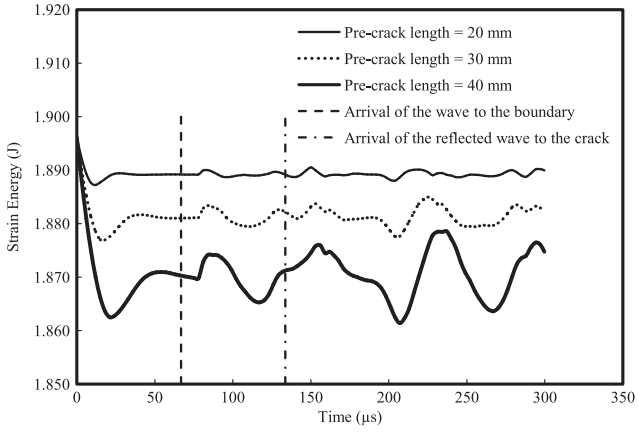

Fig. 9. Strain energy of models with different pre-crack lengths (crack propagation not allowed).

lengths of two models at different times are coincident with each other. The released strain energies are also plotted in the same figure, and from the figure, a significant difference can be observed. The ratio between the released energy is 0.25 (square of the ratio of the far-field loading). From geometric scaling, the ratio between the intrinsic fracture energy release rate of the two models is also 0.25. From the numerical results, we can also conclude that for self-similar crack growth, the loading parameter should be treated as a model constant rather than the fracture energy release rate or intrinsic fracture release rate.

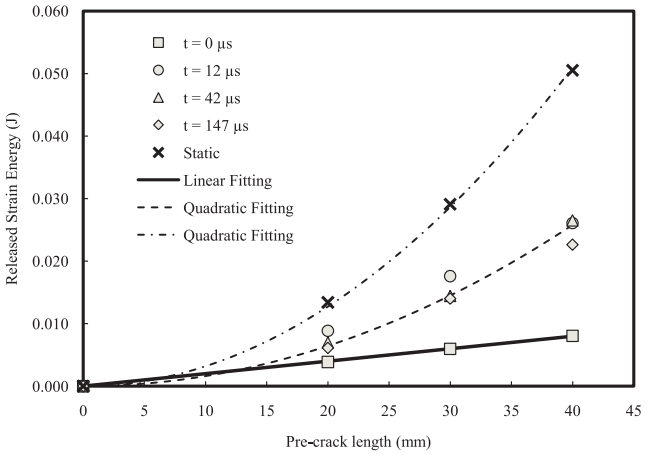

Fig. 10. Relationship between the released strain energy and the pre-crack length.

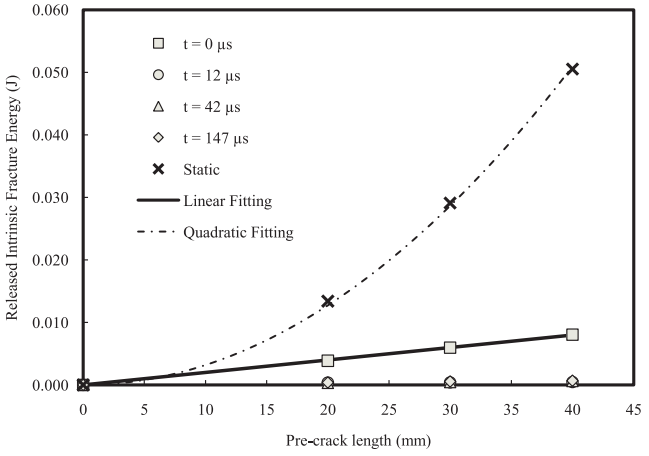

Fig. 11. Relationship between the released intrinsic fracture energy and the pre-crack length.

4.3. Crack tip damage zone and crack branching

In the experimental observation, a damage zone exists around the crack tip of the self-similar crack growth. It was considered that the change in the size of the damage zone is the reason for the increase in the fracture energy [32]. In the numerical simulation, similar phenomena are also observed. For the model shown in Fig. 4, when the time exceeds 72 μs, a damage zone is observed around the crack tip (Fig. 15a). The increase in the damage zone of dynamic fracture has been observed in experiments and numerical simulations. For example, James Rice demonstrated this phenomenon using numerical simulation of a mode-II dynamic fracture [9]. The physical reason for the increase in the damage zone is that extra strain energy is available to drive the crack, and if the crack velocity remains the same, then the increase in damage is the only possible way to consume such energy.

This damage zone further leads to crack branching, as shown in Fig. 15b and c. However, this damage zone might not be the reason for the constant crack speed. As shown in Fig. 16, the crack half-length (mapped in the x direction) remains nearly unchanged before and after crack branching. Therefore, according to the numerical simulation, the damage zone or the change in the failure pattern does not influence the numerically observed crack speed.

The above observation is consistent with the self-similar crack growth theory. When the observer moves away from the centre point, any branching or damage zone becomes negligible in size, and thus, the fracture can still be treated as a straight line.

In fact, self-similarity is expected for an ideal crack based on the assumption that the crack path is one-dimensional. This assumption is reasonable because the width of the damage zone is negligible

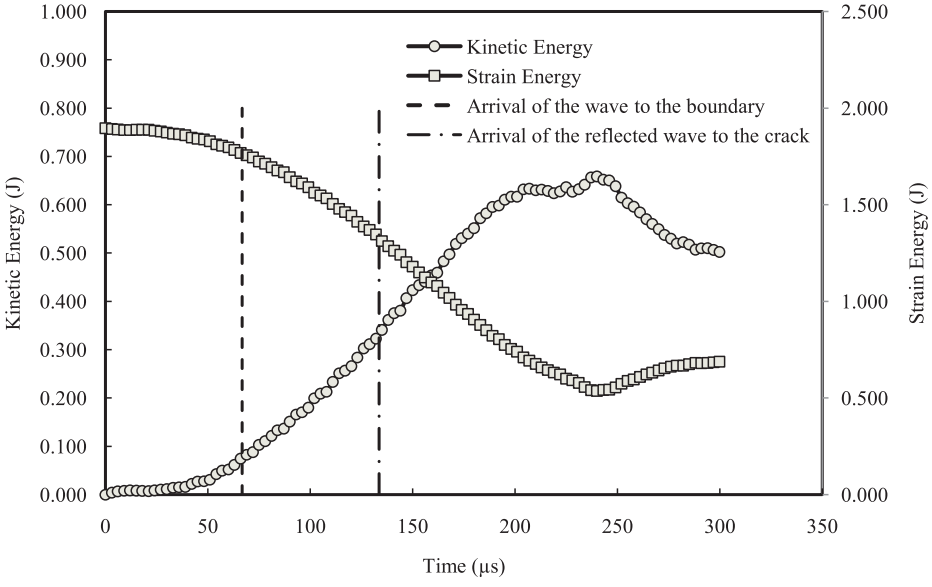

Fig. 12. Kinetic and strain energy of a model with a pre-crack length of 20 mm when crack propagation is allowed.

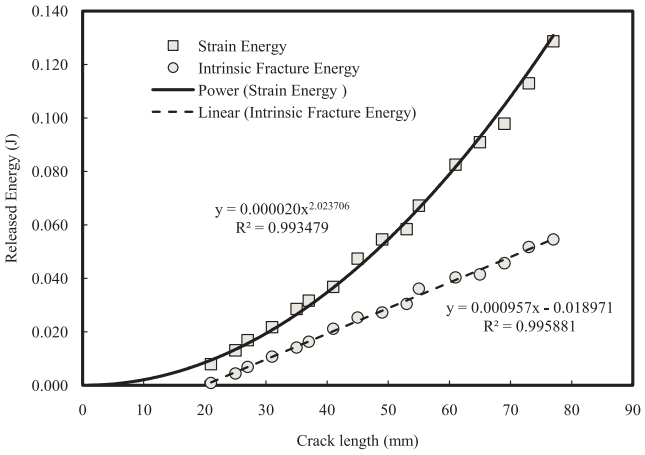

Fig. 13. Relationship between the released strain energy, intrinsic fracture energy and crack length (the pre-crack length is 20 mm).

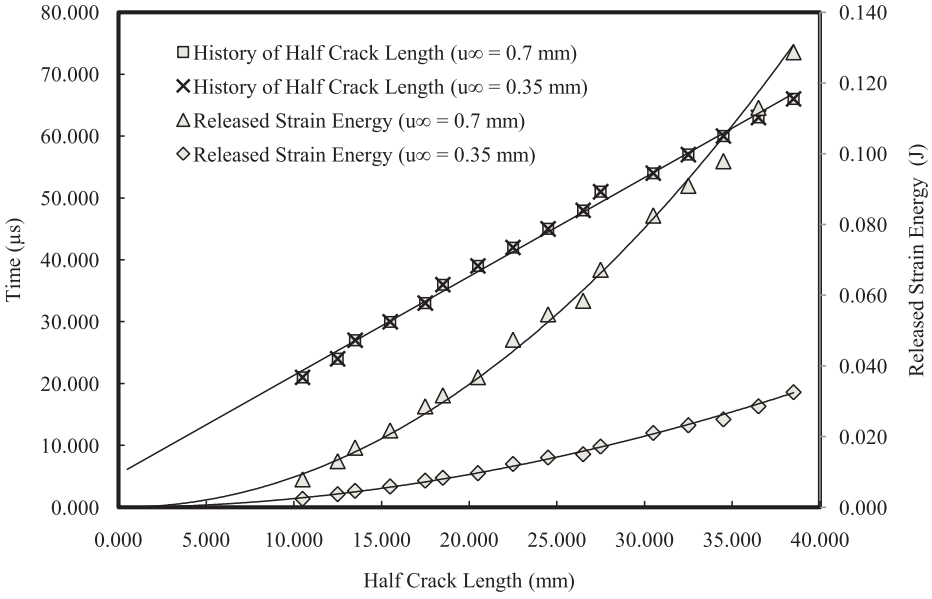

Fig. 14. Results of the half-crack length and the released strain energy of two models with different far-field loading.

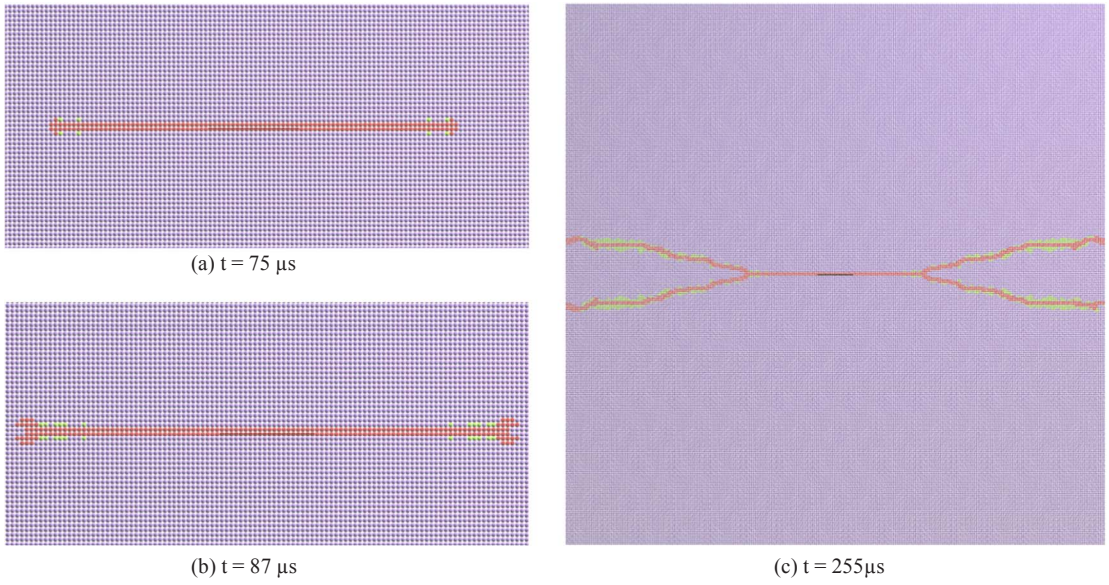

Fig. 15. Damage zone around the crack tip and crack branching.

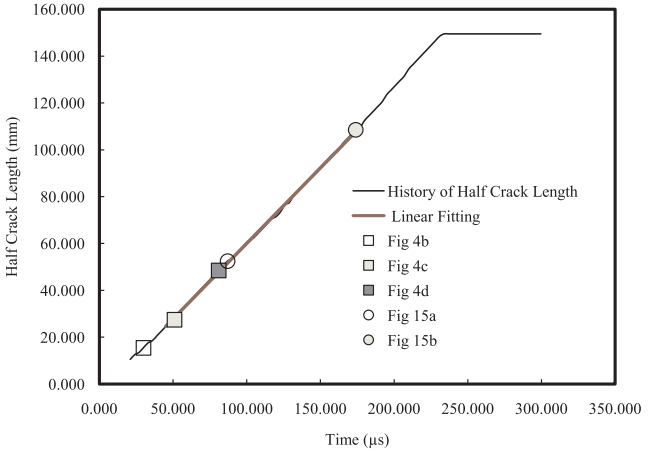

Fig. 16. Half-crack length in the *x* direction for "self-similar" crack growth considering the damage zone around the crack tip and crack branching.

compared with the crack length. The similarity of the crack growth is thus not broken, and this fact was confirmed by the discrete simulation conducted in this work.

In our numerical simulation of the self-similar crack propagation, the initial intrinsic fracture energy is linear with pre-crack length due to the cutting procedure removes the spring bonds together with the stored strain energy. This amount of energy will trigger the strain energy redistribution within the cracked body and kinematic energy as well. Because large portion of this trigger energy turns into kinetic energy, the intrinsic fracture energy during self-similar crack growth is actually relatively small compared with the strain energy released under static loading condition. From further analysis, the numerically observed fracture energy increase is also found to be irrelevant to the enlargement of the damage zone around the crack tip. Therefore, we concluded that the fracture energy increase is a result of natural process in the self-similar crack growth: that is the kinetic and strain energy redistribution.

5. Conclusions

In this work, the DLSM is used to study "self-similar" crack growth. In a comparison between the numerical simulation and the corresponding theoretical and experimental results, the DLSM is found to be able to reproduce the essential information of self-similar crack growth, such as the relationship between the crack speed and the loading parameter. Moreover, the dynamic stress intensity factor and fracture energy release are also successfully captured by the DLSM. Finally, it is concluded that the fracture energy increase in self-similar crack growth is a macroscopic result of the meso-scale spring bond breakage-induced kinetic and strain energy redistribution. The damage zone and crack branching might not be the reason for the fracture energy increase. Obtaining a deeper understanding of the physics of self-similar growth is the main purpose of this work. To this end, the DLSM appears to be a useful tool for further exploration of the physics of self-similar crack growth.

Acknowledgments

This research is financially supported by National Natural Science Foundation of China (Grant No. 1177020290).

References

[1] Abraham FF. Unstable crack motion is predictable. J Mech Phys Solid 2005;53(5):1071–8.
[2] Andrews DJ. Rupture dynamics with energy loss outside the slip zone. J Geophys Res-Sol Ea 2005;110:B01307.
[3] Beebe WM. An experimental investigation of dynamic crack propagation in plastic and metals, Air Force Materials Laboratory Technical Report; 1966.
[4] Broberg KB. The propagation of a brittle crack. Ark Fys 1960;18:159–92.
[5] Broberg KB. Cracks and fracture. San Diego: Academic Press; 1999.
[6] Burridge R, Willis JR. Self-similar problem of expanding elliptical crack in an anisotropic solid. Proc Camb Philos S-M 1969;66:443–68.
[7] Cundall PA, Strack ODL. Discrete numerical model for granular assemblies. Geotechnique 1979;29(1):47–65.
[8] Das S, Boatwright J, Scholz CH. Earthquake source mechanics, geophysical monograph, vol. 37. Washington: American Geophysical Union; 1988. p. 341.
[9] Falk ML, Needleman A, Rice JR. A critical evaluation of dynamic fracture simulation using cohesive surfaces. J de Phys IV Proc 2001:43–50.
[10] Freund LB. Crack-propagation in an elastic solid subjected to general loading. 1. Constant rate of extension. J Mech Phys Solids 1972;20:129–40.
[11] Freund LB. Crack-propagation in an elastic solid subjected to general loading. 2. Nonuniform rate of extension. J Mech Phys Solids 1972;20:141–52.
[12] Freund LB. Crack-propagation in an elastic solid subjected to general loading. 3. Stress wave loading. J Mech Phys Solids 1973;21:47–61.
[13] Freund LB. Crack-propagation in an elastic solid subjected to general loading. 4. Obliquely incident stress pulse. J Mech Phys Solids 1974;22:137–46.
[14] Freund LB. Dynamic fracture mechanics. New York: Cambridge University Press, Cambridge; 1990.
[15] Gao HJ. A theory of local limiting speed in dynamic fracture. J Mech Phys Solids 1996;44:1453–74.
[16] Hrennikoff A. Solution of problems of elasticity by the framework method. ASME J Appl Mech 1941;8:A619–715.
[17] Jing L. A review of techniques, advances and outstanding issues in numerical modelling for rock mechanics and rock engineering. Int J Rock Mech Min 2003;40:283–353.
[18] Johnson E. Process region changes for rapidly propagating cracks. Int J Fract 1992;55:47–63.
[19] Johnson E. Process region influence on energy-release rate and crack-tip velocity during rapid crack-propagation. Int J Fract 1993;61:183–7.
[20] Kazerani T, Zhao G-F, Zhao J. Dynamic fracturing simulation of brittle material using the Distinct Lattice Spring Model (DLSM) with a full rate-dependent cohesive law. Rock Mech Rock Eng 2010;43:717–26.
[21] Kostrov BV, Das S. Principles of earthquake source mechanics. Cambridge, New York: Cambridge University Press; 1988.
[22] Ling Z, Shen L. Microcracks propagation in one Al/SiCp under impact loading. J Phys IV 2006;134:957–64.
[23] Poliakov ANB, Dmowska R, Rice JR. Dynamic shear rupture interactions with fault bends and off-axis secondary faulting. J Geophys Res-Sol Ea 2002;107:2295.
[24] Ravichandar K, Knauss WG. An experimental investigation into dynamic fracture: III. On steady-state crack-propagation and crack branching. Int J Fracture 1984;26:141–54.
[25] Ravichandran G, Clifton RJ. Dynamic fracture under plane-wave loading. Int J Fracture 1989;40:157–201.
[26] Rosakis AJ, Duffy J, Freund LB. The determination of dynamic fracture-toughness of Aisi 4340 steel by the shadow spot method. J Mech Phys Solids 1984;32:443–60.
[27] Silling SA. Reformulation of elasticity theory for discontinuities and long-range forces. J Mech Phys Solids 2000;48:175–209.
[28] Silling SA, Weckner O, Askari E, Bobaru F. Crack nucleation in a peridynamic solid. Int J Fract 2010;162. 219-217.
[29] Slepyan LI, Ayzenberg-Stepanenko MV. Some surprising phenomena in weak-bond fracture of a triangular lattice. J Mech Phys Solid 2002;50:1591–625.
[30] Willis JR. Self-similar problems in elastodynamics. Philos Trans R Soc A 1973;274:435–91.
[31] Xia K, Chalivendra VB, Rosakis AJ. Spontaneous mixed-mode fracture in bonded similar and dissimilar materials. Exp Mech 2006;46:163–71.
[32] Xia K, Liu C, Kanopoulos P. On the energy of dynamic fractures. Int J Nonlin Sci Numer 2012;13:117–22.
[33] Xia KW, Chalivendra VB, Rosakis AJ. Observing ideal "self-similar" crack growth in experiments. Eng Fract Mech 2006;73:2748–55.
[34] Xia KW, Rousseau CE, Rosakis A. Experimental investigations of spontaneous bimaterial interfacial fractures. J Mech Mater Struct 2008;3:173–84.
[35] Yoffe EH. The moving Griffith crack. Philos Mag 1951;42:739–50.
[36] Zhang X-P, Wong LNY. Crack initiation, propagation and coalescence in rock-like material containing two flaws: a numerical study based on bonded-particle model approach. Rock Mech Rock Eng 2013;46:1001–21.
[37] Zhao G-F. Developing a four-dimensional lattice spring model for mechanical responses of solids. Comput Meth Appl Mech Eng 2017;315:881–95.
[38] Zhao G-F, Fang J, Zhao J. A 3D distinct lattice spring model for elasticity and dynamic failure. Int J Numer Anal Met 2011;35:859–85.